IEEE Access
Multidisciplinary ⋮ Rapid Review ⋮ Open Access Journal

Received December 13, 2021, accepted January 3, 2022, date of publication January 25, 2022, date of current version January 31, 2022.

Digital Object Identifier 10.1109/ACCESS.2022.3145239

Impact Assessment of Energy Storage Systems Supporting DC Railways on AC Power Grids

G. GRABER, (Member, IEEE), V. CALDERARO, (Senior Member, IEEE), V. GALDI, (Senior Member, IEEE), L. IPPOLITO, AND G. MASSA, (Member, IEEE)
Department of Industrial Engineering (DIIn), University of Salerno, 84084 Fisciano, Italy

Corresponding author: V. Calderaro (vcaldeararo@unisa.it)

This work was supported by the National Operative Program Research and Competitiveness (R&C) of Italian Ministry of University and Research through the Research Project NEMBO: iNnovative EMBedded systems for railway applicatiOns.

ABSTRACT Energy storage systems (ESSs) represent an established solution for energy saving and voltage regulation in DC urban railway systems. In particular, ESSs can store the braking energy of light rail vehicles (LRVs) and support the DC feeder system during traction operations. Moreover, ESSs can significantly improve the operating conditions of the AC supply system by reducing voltage drops and current spikes. This paper investigates the impact on the bus voltages and branch currents of the AC grid of wayside and on-board ESSs supporting the DC railway infrastructure. An iterative algorithm solves the decoupled AC/DC power flow considering the 3-phase bridge rectifier model of traction substations. The work presents a novel mathematical formulation of the optimization problem to solve the positioning and sizing of supercapacitor-based wayside ESSs, considering both DC and AC network constraints. The effectiveness of the proposed method is proved through numerical simulations on a real Italian DC railway system. Obtained results are presented and discussed comparing the proposed methodology to several existing literature solutions.

INDEX TERMS AC power grid, AC/DC load flow, energy storage system, railway system simulation, supercapacitors.

I. INTRODUCTION

Up to 2050, passenger mobility will increase by 300%, as stated by the International Transport Forum [1]. Thus, smart solutions to provide adequate transport capacity for growing volumes of people and goods have to be implemented, mitigating energy consumption and pollution emissions [2]. Nowadays, the significant deployment of mass transport systems using the electric energy carrier in urban and metropolitan areas, such as subways, trams and light rail, provides both a sustainable mobility solution and a possible alternative to private vehicles [3].

However, the railway sector is not resting at evaluating the energy efficiency advantage compared to other transport modes but aims at improving technologies that can increase its convenience [3], [4]. In particular, research activities mainly focus on the development of more efficient design techniques for drivetrains, eco-drive speed profiles (i.e. driving cycles able to minimize the energy consumption during the journey), and regenerative braking energy saving methods [4]. Energy storage systems (ESSs) represent a promising solution because they can store the braking energy of light rail vehicles (LRVs) and support the DC feeder system during traction operations [5], [6]. The pantograph-overhead line provides continuous power for LRV operations, whereas wayside and/or on-board ESSs serve as auxiliary power supply [7], [8]. Even if the energy efficiency increasing itself could be a valid reason to install ESSs along DC railway systems, additional benefits could be provided by these technologies [9]–[11]. Indeed, ESSs can mitigate high voltage drops caused by an increase of the service level (number of rides within a given time period) or by the introduction of new modern and powerful LRVs [5], [6]. Moreover, ESSs reduce power losses along the track as well as the rating of the traction power substation (TPS) rectifier power devices by lowering the LRV peak power absorption [9]–[11]. ESSs also have a significant impact on reliability; indeed, they help to slow down the aging effect affecting TPS power

The associate editor coordinating the review of this manuscript and approving it for publication was Alon Kuperman.

components (transformer mainly) by reducing the overloading of the track power line and substation. Finally, ESSs characterized by large energy reserves can also become an off-grid traction power supply during emergency operating conditions [11].

In the urban railway system, ESSs can be installed near the TPS or along the track as well as on-board the LRV. Compared to on-board energy storage systems (OBESS), wayside ones are not subject to weight and size constraints imposed by the vehicle. Several ESSs based solutions have been proposed by scientific literature: lithium batteries, supercapacitors (SC), and flywheels [12]–[14]. Among them, SC and flywheels-based ESSs are the most attractive ones due to their high specific power, the large number of charging and discharging cycles, and the expected future advances of these technologies [15]. Several papers have been produced on the implementation of wayside ESSs [12], [13], [15]–[19]. In particular, a SC-based substation for voltage drops compensation in light rail networks is investigated in [12] while [15] has proposed a control strategy for wayside SC-based systems implementing the real-time management of voltage levels at catenary connection points. In [16], the first results of the Li-ion battery system installed at HAIJIMA Substation (SS) on the Ome Line have been presented, while [13] has analyzed the potential benefits of flywheel energy storage for dc light rail networks. In [17] the Authors have investigated the joint siting and sizing procedure of wayside SCs in urban rail transit by optimizing the energy supplied by the TPSs. In [18], the East Japan Railway Company has described the effects of three energy storage systems installed along the traction power supply infrastructure.

However, railway DC feeder systems produce harmonic distortion and voltage unbalance on the local distribution AC network [19]. The harmonic distortion is caused by non-linear currents drawn by the railway DC system through the rectifying substations [19], [20]. In detail, voltage unbalance is present in AC systems when the DC feeder system draws large currents from a single phase of the AC supply network [21], [22]. On the other side, distribution network operators specify power quality standards to be met by railway systems [23]. Thus, ESSs installed along the track or supporting the TPS could be also beneficial to the AC supply system. In particular, they could improve the AC operating conditions by reducing peak values of absorbed current and voltage drops and by mitigating the negative impact of the railway system on other users connected to the same AC power grid [24]. The manager of the railway infrastructure could also be interested in installing ESSs because they reduce high electricity bills due to peak power absorptions [26]. Finally, if the TPS is reversible, ESSs could become a smart grid asset capable of providing power in emergency conditions or demand response services to the local energy distribution company [11], [27].

For these reasons, it is important to evaluate the impact of the railway feeder system on the local distribution network to quantify the benefit introduced by wayside ESSs. Thus, a new design of the whole light railway power supply network from the AC supply to the DC network is needed.

This paper investigates the impact of wayside SC-based ESSs (supporting the DC railway system) on bus voltages and branch currents of the AC power grid. The key contributions of this paper are summarized as follows: i) it describes a decoupled methodology to solve DC traction power flow with integrating ESSs, developing an overall framework that includes the AC distribution network model; ii) it introduces a novel mathematical formulation of the optimization problem concerning positioning and sizing of SC-based ESSs, taking into account DC and AC network requirements and constraints; iii) it proposes a sensitivity analysis of the AC power grid for different positioning and sizing design cases concerning the ESS. Finally, it evaluates the benefits produced by ESSs on the AC network, through numerical simulations performed on a real Italian DC railway system.

The remainder of the paper is organized as follows: Section II describes the electrical models of the DC feeder system, including LRV, SC-based ESS, and 3-phase bridge rectifier implemented within the railway network simulator. Section III introduces the AC/DC power flow algorithm, whereas the proposed positioning and sizing optimization algorithm for wayside ESSs is described in Section IV. Finally, numerical results are presented and discussed in Section V, with concluding remarks listed in Section VI.

II. THE DC FEEDER SYSTEM

The existing equivalent circuits for the ESS modelling in DC railway feeder systems are extended to include both wayside ESSs and on-board ESSs, taking into account the related DC/DC power converter and its current control characteristics, too. In addition, the equivalent circuit of the three-phase rectifier is integrated to extend the modelling of the DC feeder system up to the AC distribution network and to evaluate the positive effects of the ESSs, taking into account active and reactive power consumption of the TPS.

The proposed methodology aims at being a helpful tool for engineers and technicians during feasibility analysis or preliminary design phases to study power flows involving the DC network and AC grid to compare different ESSs sizing and positioning solutions. Thus, quasi-static equivalent models for LRVs, ESSs and feeder systems are used. Indeed, accurate and more complex models able to describe electric transient states are not helpful for our scope. In addition, simplified models are required to reduce the computing time of the ESS sizing and positioning algorithm described in Section IV, which requires to solve an iterative algorithm for AC-DC power flow at each time step of the track simulation.

However, kinematic and electric models, used to describe DC railway systems, depend on several parameters (i.e., wheel-rail friction coefficients, catenary resistive coefficients, powertrain components efficiencies, etc.). Their values are often not known accurately. The uncertainty related to these parameters is due to several factors, such as

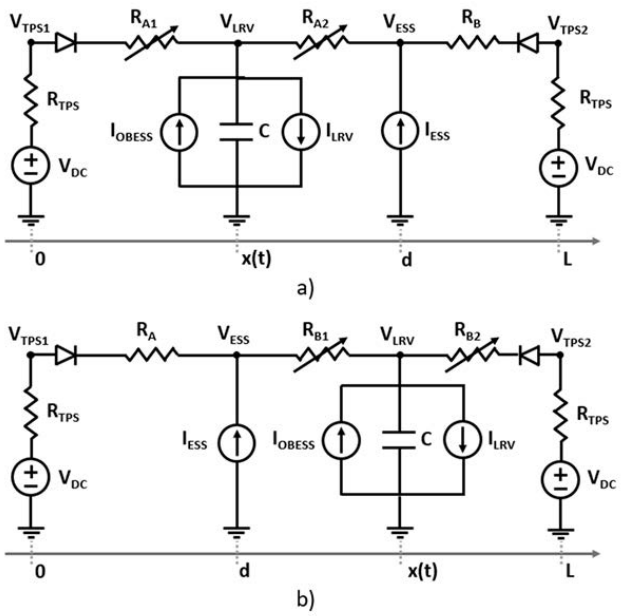

FIGURE 1. Electric model of the double side fed DC railway system: a) one LRV equipped with OBESS positioned before the wayside ESS, and b) after the wayside ESS.

infrastructure deterioration or aging, inaccurate measurements, neglected phenomena in the used model, etc.

For these reasons, measured data are required to validate models and simulators. Thus, present work uses measured data obtained during experimental tests carried out as part of the activities related to the research project *NEMBO - iNnovative EMBedded systems for railway applicatiOns*, funded by the national Operative Program R&C of the Italian Ministry of University and Research.

Starting from measured data, a calibration methodology to derive the value of the model parameters is used, thus validating the DC railway systems simulator. It works by finding the parameter values that minimize the error between the measured energy data and the one computed by the proposed model, at specific points over time [25]. In this paper, typical or measured (when they are available) values of such parameters to test the proposed methodology on a real case study are used.

A. THE DC POWER FLOW

The electric model of a double-side fed DC contact line, equipped with a single ESS along the track and one LRV, is shown in Fig. 1. The TPS, like most of the conventional substations, is not reversible and can be modelled as an ideal voltage source V_{DC} in series with a resistor R_{TPS} and an ideal diode [19], [28]. Contrariwise, within this work, LRVs are modeled as ideal current sources: I_{LRV} value is computed as the ratio between the LRV electric power P_{LRV}, and the line voltage at the LRV position, V_{LRV}, changing along the track. ESSs are represented as ideal current sources because they support the feeder system during the traction phase of LRVs storing regenerative braking energy. In particular, the OBESS model is parallel to the LRV model, while the wayside ESS model is considered as a node of the DC feeder system. The State of Charge (SoC) variation according to the ESS/OBESS current is calculated by using the electric models of the storage modules (batteries, SC, etc.) and the DC/DC power converter with its controller. Moreover, a small capacitance C, in parallel to the ideal current source, is added in the LRV model to describe the receptivity of the network under regenerative braking conditions, [6], [17]. It refers to the line voltage rise during the regenerative braking, which is used by the ESS control system to detect a braking vehicle along the track.

The overhead line is modelled by a set of electric resistances that change their value according to the LRV position. If $x(t)$ represents the LRV position at time t, the values of the upstream (R_{A1}) and downstream (R_{A2}) resistance to the LRV towards a generic node of the railway feeder system (TPS, ESS, or another train) are calculated by:

$$\begin{cases} R_{A1}(t) = \rho \cdot x\,(t) \\ R_{A2}(t) = \rho \cdot [d - x\,(t)] \end{cases} \tag{1}$$

where ρ is the resistive coefficient, and d is the distance between the couple of nodes placed upstream and downstream with respect to the LRV, according to the axis origin highlighted in Fig. 1. For feeder systems with overhead line supply conductors and a rail current flow return, the return resistance is lumped with the supply resistance introducing an error less than 3% [13].

Finally, nodal analysis is implemented to determine unknown voltages on the DC network [13], [29]. More in detail, by applying Kirchhoff's current law, the feeder system is described by a set of $2n$ linear equations, where n are the nodes of the DC network. In particular, assuming a double-fed DC feeder system and one LRV before one ESS on the track (Fig. 1 a), it is possible to calculate the V_{LRV} and the line voltage at the ESS position, V_{ESS} by solving (2).

$$\begin{cases} \dfrac{V_{DC} - V_{LRV}(t)}{R_{TPS} + R_{A1}} + I_{ESS}\,(t) + \dfrac{V_{DC} - V_{ESS}(t)}{R_{TPS} + R_B} \\ = \dfrac{P_{LRV}(t)}{V_{LRV}(t)} - I_{OBESS}\,(t) + C\dfrac{dV_{LRV}}{dt} \\ \dfrac{V_{LRV} - V_{ESS}(t)}{R_{A2}} + \dfrac{V_{DC} - V_{ESS}(t)}{R_{TPS} + R_B} = -I_{ESS}\,(t) \end{cases} \tag{2}$$

where P_{LRV} is the LRV electric power requested/injected to the feeder system and I_{ESS} is the current supplied/absorbed by the ESS (both parameters are given). Equation (2) is a non-linear second order differential equation set with V_{LRV} and V_{ESS} unknowns. However, by using the finite difference

method, it is possible to rewrite (2) as:

$$\begin{cases} \dfrac{V_{DC} - V_{LRV}(k)}{R_{TPS} + R_{A1}} + I_{ESS}(k-1) + \dfrac{V_{DC} - V_{ESS}(k)}{R_{TPS} + R_B} \\ = \dfrac{P_{LRV}(k)}{V_{LRV}(k)} - I_{OBESS}(k-1) \\ \quad + C\dfrac{V_{LRV}(k) - V_{LRV}(k-1)}{\Delta T} \\ \dfrac{V_{LRV} - V_{ESS}(k)}{R_{A2}} + \dfrac{V_{DC} - V_{ESS}(k)}{R_{TPS} + R_B} = -I_{ESS}(k-1) \end{cases} \tag{3}$$

where $V_{LRV}(k)$ is the V_{LRV} value during the k-th time step. During each $k \cdot \Delta T$, by using the substitution method, it is possible to solve the linear second order equation set (3), re-written in general form as follows:

$$\begin{cases} a_1 V_{LRV}^2 + a_2 V_{LRV} + a_3 V_{LRV} V_{ESS} + a_4 = 0 \\ b_1 V_{LRV} + b_2 V_{ESS} + b_3 = 0 \end{cases} \tag{4}$$

where:

$$\begin{cases} a_1 = \left(1 + \dfrac{C}{\Delta T} \cdot a_3\right) \cdot b_1 \\ a_2 = -\left(\left(I_{ESS}(k-1) + \dfrac{C}{\Delta T} V_{LRV}(k-1)\right) \right. \\ \qquad \left. \cdot a_3 \cdot b_1 + V_{DC} \cdot (a_3 + b_1)\right) \\ a_3 = (R_{TPS} + R_{A1}) \\ a_4 = P_{LRV}(k) \cdot a_3 \cdot b_1 \end{cases}$$

$$\begin{cases} b_1 = (R_{TPS} + R_B) \\ b_2 = -(b_1 + R_{A2}) \\ b_3 = (V_{DC} + I_{ESS}(k-1) \cdot b_1) \cdot R_{A2} \end{cases} \tag{5}$$

The positive root among those ones of the quadratic equation according to the initial conditions, $P_{LRV}(0) = 0\, I_{ESS}(0) = 0$, $I_{OBESS}(0) = 0$, $C = 0$ are chosen, where the solution has to be $V_{LRV}(0) = V_{DC}$. Similar results can be obtained with other configurations: i.e. LRV positioned after the ESS (Fig. 1b) or more than one ESS/LRV on the track at the same time.

B. THE LRV

The LRV longitudinal dynamic behaviour is described by using the mass-point model, [6], [18], [28], [29], according to Newton's second law and to the following kinematics equations:

$$\begin{cases} m\dfrac{dv}{dt} = F_{mech}(t) - R_{BASE}(v) - R_{LINE}(x) \\ x = x_0 + v_0 t + \dfrac{1}{2}\dfrac{dv}{dt}t^2 \end{cases} \tag{6}$$

where v and x are the speed and position of the train, respectively, and $F_{mech}(t)$ is the mechanical traction/braking force. The effective mass of the train $m = [(1+\varepsilon) \cdot m_T] + m_L$ is computed by increasing its empty mass (m_T) by a factor ε to take into account the rotating mass effect, and by adding the load mass of passengers (m_L). $R_{BASE}(v)$ is the basic resistance associated to roll resistance and aerodynamic drag, while

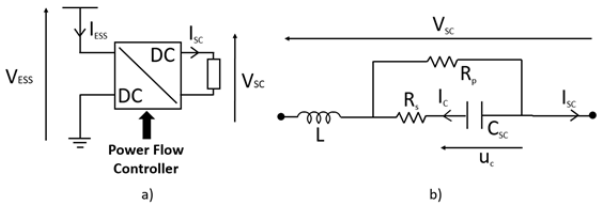

FIGURE 2. a) ESS main components. b) SC first order equivalent circuit.

$R_{LINE}(x)$ is the line resistance depending on track slopes and curves, [6], [10], [13]. They are computed by:

$$\begin{aligned} R_{BASE} &= \alpha_1 + \alpha_2 |v| + \alpha_3 v^2 \\ R_{LINE} &= mg \sin(\gamma(x)) + mg\frac{a}{r(x) - b} \end{aligned} \tag{7}$$

In (7), α_1, α_2, and α_3 are the coefficients of the Davis formula, related to the train and the track characteristics; they can be calculated by empirical measures, or obtained by literature works [10], [28]. The curve resistance - the second term of R_{LINE} - is given by empirical formulas, as Von Röckl's one, where $r(x)$ is the curvature radius; a, b parameters depend on the track gauge [28]. Finally, $\gamma(x)$ is the slope grade, and g is the gravitational acceleration. Starting from the LRV speed profile along the track, the tractive effort at the wheels, F_{mech}, is computed by using (6) and (7) and taking into account the boundary of the LRV traction/braking curve. By using the efficiency parameters of the train components, P_{LRV} is calculated as follows:

$$P_{LRV} = \begin{cases} \dfrac{F_{mech} v}{\eta_g \eta_m \eta_i} + P_{SERVICES} & F_{mech} \geq 0 \\ (F_{mech} v) \cdot \eta_g \eta_m \eta_i + P_{SERVICES} & F_{mech} < 0 \end{cases} \tag{8}$$

where $P_{SERVICES}$ is the required power for auxiliary services (e.g. lighting and air conditioning), η_g represents the gear system efficiency, η_i is the average value of the inverter efficiency, while η_m describes the induction motor efficiency, expressed in [28] as follows:

$$\eta_m = \frac{P_{out}}{P_{out} + loss} = \frac{T\omega}{T\omega + k_c T^2 + k_i \omega + k_w \omega^3} \tag{9}$$

In (9), $T = F_{mech} \cdot r_{wheel}/n_{motor\_axles}$ and $\omega = v/r_{wheel}$ are the mechanical torque required by each motored axle and the angular speed, respectively, while r_{wheel} is the wheel radius and n_{motor_axles} is the number of motored axles. The term $k_c \cdot T^2$ describes the copper losses caused by the electrical resistance of the motor wires, $k_i \cdot \omega$ represents the iron losses taking into account both hysteresis and eddy current effects in the iron rotor, and $k_w \cdot \omega^3$ represents the windage losses due to friction and wind resistance of the rotor [30]. The values of the coefficients k_c, k_i, k_w are typically found by regression using measured values of efficiency.

C. SC-BASED ESSs

Ideal current sources represent wayside ESSs and OBESS. Electric models of SC modules and DC/DC power converter with its controller are used to calculate the state of

charge (SoC) variation related to the value of the ESS/OBESS current. In particular, Fig. 2a shows the input and output voltages of the DC/DC converter: V_{ESS} is the voltage of the DC network where the ESS is installed (for wayside ESS) or the LRV voltage (for on-board ESS), whereas V_{SC} is the voltage of the SC modules described by Eq. (10). In detail, the OBESS representation can be obtained by replacing V_{ESS} with $V_{OBESS} = V_{LRV}$ and I_{ESS} with I_{OBESS}. When the ESS/OBESS has to recover the braking energy, the DC/DC converter works in step-down mode, with V_{ESS} being its input and V_{SC} its output. On the other hand, when the ESS has to support the feeder system, the DC/DC converter works in step-up mode, with V_{SC} as its input and V_{ESS} as its output. Moreover, Fig. 2b shows the first-order equivalent circuit of an SC module consisting of four elements [10], [16], [13]. The series resistance R_s describes the power loss during the charging and discharging operations while the inductance L results mainly from the SC physical construction and its value is usually negligible. The self-discharge resistance R_p models the losses due to the leakage current, while the capacitor C_{SC} (modelling the SC's capacity) changes linearly with the SC electrodes voltage, V_{SC}. The equation set (10) summarizes the SC electrical model.

$$\begin{cases} V_{SC}(t) = u_C(t) - R_S I_C(t) \\ u_C(t) = u_C(t=0) + \dfrac{1}{C_{SC}} \displaystyle\int_0^t I_C(\tau)\, d\tau \\ I_C(t) = I_{SC}(t) - \dfrac{1}{R_P}\left(u_C(t) - R_S I_C(t)\right) \\ C_{SC} = C_0 \cdot [1 + \lambda V_{SC}(t)] \end{cases} \tag{10}$$

Specifically, the first equation represents Kirchhoff's voltage law, while the second one is the ideal capacitor current-voltage relationship. The third equation is Kirchhoff's current law, and finally, the last equation models the SC's capacity variation law. In (10), $I_{SC}(t)$ is the SC current, C_0 is the base capacity, and λ [V^{-1}] represents the SC capacity voltage coefficient. Finally, the SoC of the SC module is computed by:

$$SoC_{SC}(t) = \frac{V_{SC}^2(t)}{V_{SC}^2(t=0)} \tag{11}$$

Through a similar approach used for the DC feeder, the V_{sc} value is obtained by discretizing and solving equations (10) and (11), considering given the I_{SC} value. Both wayside and on-board ESSs are connected to the DC feeder system through a DC/DC power converter with a current feedback control loop. The DC/DC power converter is modelled by its average efficiency η, describing power losses [18], [29]. It operates as a step-up or step-down converter according to its required operating mode. In particular, given the current reference value I_{ESS} (provided by the control characteristic of the power converter), the related SC current value is computed by using (12).

$$I_{SC} = \frac{1}{\eta}\frac{V_{ESS}}{V_{SC}} I_{ESS} \tag{12}$$

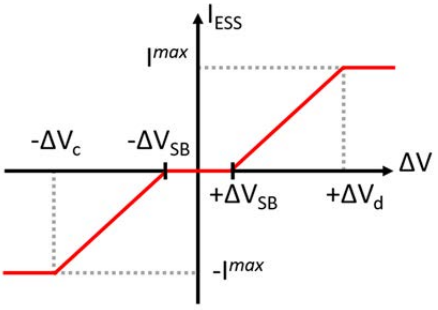

FIGURE 3. Control characteristic of the DC/DC converter interfacing the SC-based ESS to the DC feeder system.

Equation (12) can be extended to OBESSs by replacing V_{ESS} with V_{OBESS} and I_{ESS} with I_{OBESS}. Fig. 3 illustrates the ESS control characteristic: it is the linear relationship between the reference current of the ESS I_{ESS} (in step-up or step-down mode) and the voltage difference ΔV between the feeder voltage V_{ESS} with no LRVs on the track, and its current value. In detail, if the voltage difference is positive ($\Delta V > 0$), it means that one or more LRVs are in traction mode on the track, reducing the feeder voltage; thus, the ESS has to support the DC network by discharging itself ($I_{ESS} > 0$). If the voltage difference is negative ($\Delta V < 0$), it means that one or more LRVs are in the regenerative braking phase, injecting power in the DC network, increasing the feeder voltage as a result. For this reason, the ESS has to absorb power from the DC network ($I_{ESS} > 0$). Moreover, ΔV values within the $[-\Delta V_{SB}, \Delta V_{SB}]$ range represent a standby region where no actions are required. The ESS is ready to supply/recover energy and it is more or less responsive according to the charging/discharging slopes of the ESS control characteristic defined by the ΔV values $(-\Delta V_c, +\Delta V_d)$, for which the ESS shows its maximum charging/discharging current, I^{max}.

D. 3-PHASE BRIDGE RECTIFIER

Assuming $|V_{ll}|$ and ϑ the rms value and phase angle of the AC line voltage, terminal equations of the 3-phase bridge rectifier are reported as follows, where the apex pu means that the quantities are expressed in per-unit system [31].

$$\begin{cases} E_d^{pu} = \left|V_{ll}^{pu}\right| \cdot \varphi(\alpha, \mu) - R_{eq}^{pu} \cdot I_d^{pu} \\ I_d^{pu} = \dfrac{6 \cdot \left|V_{ll}^{pu}\right|}{\pi \cdot X_C^{pu} \cdot \left(1 + e^{-\lambda\mu}\right)} \cos(\xi) \\ \qquad\qquad \cdot \left[e^{-\lambda\mu}\cos(\xi + \alpha) - \cos(\xi + \alpha + \mu)\right] \\ \varphi(\alpha, \mu) = \dfrac{1}{2} \cdot [\cos(\alpha) - \cos(\alpha + \mu)] \\ \alpha = -\sin^{-1}\left(\dfrac{\pi \cdot R_C^{pu} \cdot I_d^{pu}}{6 \cdot \left|V_{ll}^{pu}\right|}\right) \end{cases} \tag{13}$$

In particular, E_d^{pu} and I_d^{pu} are the average rectifier DC output voltage and the smooth ripple-free DC load current, respectively. Moreover, α is the preignition angle for uncontrolled rectifiers or the commutation delay angle for

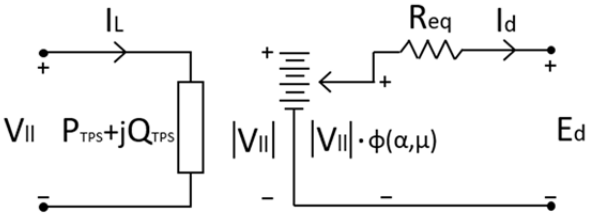

FIGURE 4. Equivalent circuit of the 3-phase bridge rectifier.

controlled rectifiers, while μ is the commutation overlap angle [31], [32]. Finally, R_C^{pu} and X_C^{pu} are the commutation resistance and reactance, respectively, while R_{eq}^{pu}, λ, and ξ are defined in (14) [31].

$$\begin{cases} R_{eq}^{pu} = \dfrac{\pi^2}{18} \cdot \left[2 - \dfrac{3\mu}{2\pi}\right] \cdot R_C^{pu} \\ \lambda = \dfrac{R_C^{pu}}{X_C^{pu}} \\ \xi = \tan^{-1}(\lambda) \end{cases} \tag{14}$$

The active and reactive power consumptions of the bridge rectifier P_{TPS}^{pu} and Q_{TPS}^{pu} are computed according to (15) [32].

$$\begin{cases} P_{TPS}^{pu} = \dfrac{3 \cdot |V_{ll}^{pu}|^2}{4\pi \cdot X_C^{pu}} \cos(\xi) \cdot A(\alpha, \mu) + \dfrac{|V_{ll}^{pu}| \cdot I_d^{pu}}{2} \cdot B(\alpha, \mu) \\ Q_{TPS}^{pu} = \dfrac{3 \cdot |V_{ll}^{pu}|^2}{4\pi \cdot X_C^{pu}} \cos(\xi) \cdot C(\alpha, \mu) + \dfrac{|V_{ll}^{pu}| \cdot I_d^{pu}}{2} \cdot D(\alpha, \mu) \end{cases} \tag{15}$$

Equations (13) and (15) allow to implement the equivalent circuit of the bridge rectifier depicted in Fig. 4, where I_L^{pu} is the AC line current expressed in (16) [31], [32].

$$\begin{aligned} I_L^{pu} = &\left[\frac{3 \cdot |V_{ll}^{pu}|}{4\pi \cdot X_C^{pu}} \cos(\xi) \cdot A(\alpha, \mu) + \frac{I_d^{pu}}{2} \cdot B(\alpha, \mu)\right] \\ &- j\left[\frac{3 \cdot |V_{ll}^{pu}|}{4\pi \cdot X_C^{pu}} \cos(\xi) \cdot C(\alpha, \mu) + \frac{I_d^{pu}}{2} \cdot D(\alpha, \mu)\right] \end{aligned} \tag{16}$$

in which:

$$\begin{cases} A(\alpha, \mu) = 2\mu \cdot \sin(\xi) + \cos(\xi + 2\alpha + 2\mu) \\ \qquad - \cos(\xi + 2\alpha) - 4\cos(\xi)\cos(\xi + \alpha) \\ \qquad \cdot \left[e^{-\lambda\mu} \cos(\xi - \alpha - \mu) - \cos(\xi - \alpha)\right] \\ B(\alpha, \mu) = \cos(\xi) \cdot \left[e^{-\lambda\mu} \cos(\xi - \alpha - \mu) - \cos(\xi - \alpha)\right] \\ \qquad - \cos(\alpha + \mu) + \cos(\alpha) \\ C(\alpha, \mu) = 2\mu \cdot \sin(\xi) + \sin(\xi + 2\alpha + 2\mu) \\ \qquad - \sin(\xi + 2\alpha) + 4\cos(\xi)\cos(\xi + \alpha) \\ D(\alpha, \mu) = -\cos(\xi) \cdot \left[e^{-\lambda\mu} \sin(\xi - \alpha - \mu) - \sin(\xi - \alpha)\right] \\ \qquad - \cos(\xi + 2\alpha) - 4\cos(\xi)\cos(\xi + \alpha) \end{cases} \tag{17}$$

III. DECOUPLED AC/DC LOAD FLOW ALGORITHM

In this Section, the proposed decoupled approach to solve the AC/DC power flow is presented, implementing an iterative procedure based on the following four phases: DC network power flow, DC/AC conversion, AC network power flow, AC/DC conversion.

A. DC NETWORK LOAD FLOW

The DC network simulator is based on the quasi-static backward-looking method and implements the electric models introduced in Sections II.A, II.B, and II.C. During each time step, the mechanical power required by the LRV to satisfy the speed cycle is determined at the wheel level; its related electric power is computed by using the efficiency parameters of each electrical LRV component [6], [13]. The DC network power flow is solved as described in Section II.A.

B. DC/AC CONVERSION

This procedure consists of computing the active and reactive power demand of the 3-phase bridge rectifier starting from the DC voltage and the current output values [32], [33]. According to the rectifier equivalent model described by (13), $|V_{ll}|$, α, and μ are unknowns variables, while E_d and I_d are constant terms. The problem is well-posed because it is composed by 3 equations and 3 unknown terms. It is a set of non-linear equations, and it can be solved by using the Levenberg-Marquardt iterative algorithm. The solution of (13) allows to compute the P_{TPS} and Q_{TPS} absorbed by the rectifier using (15).

C. AC NETWORK LOAD FLOW

AC network simulation is performed by using an AC power flow technique based on the Newton-Raphson method [34]. Constant terms and unknown variables depend on the type of bus. The railway DC network (including rectifiers) represents a bus of the AC network and it is modelled as a load bus (P_{TPS}, Q_{TPS}) [33]. In the AC network, a slack bus characterized by given values of voltage magnitude and phase, representing the high voltage AC connection point, is included [34].

D. AC/DC CONVERSION

The AC/DC conversion procedure computes the DC values of the TPS voltage and current starting from the rectifier AC input values (i.e. the solution of the AC network power flow) [33]. Using (13) to model the rectifier, the unknown variables are E_d, I_d, α, and μ, while the constant terms are $|V_{ll}|$ and I_L. In this case, the problem is not well-posed because it is composed by 3 equations and 4 unknowns. However, [31], [32] show that assuming $\mu \leq 60°$, the fundamental current component magnitude $|I_L|$ may be expressed as:

$$I_d^{pu} \cong |I_L^{pu}| \tag{18}$$

The percentage error obtained using the approximation (18) is less than 4%, [29]. Thus, (13) and (18) represent a non-linear set of equations, to be solved by using the Levenberg-Marquardt iterative algorithm again.

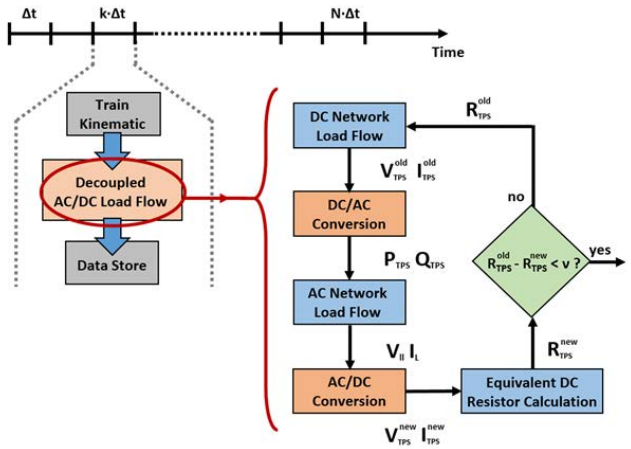

FIGURE 5. Block diagram of the decoupled AC/DC power flow algorithm.

E. AC/DC LOAD FLOW PROCEDURE

The decoupled AC/DC power flow is solved using an iterative procedure as shown in Fig. 5 [33]. It is summarized as follow:

- DC voltage and current of the TPS (V_{TPS}^{old} and I_{TPS}^{old}) are computed solving the DC network power flow.
- Active and reactive power (P_{TPS} and Q_{TPS}) at the AC side of the rectifier are determined starting from the V_{TPS} and I_{TPS} values.
- Voltage and current values at the AC side of the rectifier (V_{ll} and I_L) are computed.
- Starting from the solution of the AC power flow, new DC electrical states (V_{TPS}^{new} and I_{TPS}^{new}) are calculated.

The proposed approach computes the dummy resistance R_{TPS}, at each iteration of the AC/DC power flow procedure, considering the load effect on the AC voltage powering the TPS and the voltage drops due to the non-ideality of the rectifier. In other words, R_{TPS} represents the connecting element between the AC and DC power flow equations, defined in (19).

$$R_{TPS} = \frac{V_{DC} - V_{TPS}}{I_{TPS}} \tag{19}$$

Once achieved the convergence for the dummy resistance, (i.e. the difference between two consecutive iterations lower than a given threshold υ), the iterative procedure successfully ends providing a feasible solution that satisfies both the AC and DC equations set [31].

IV. THE ESS POSITIONING AND SIZING PROBLEM

The innovative proposed solution aims at solving the problem of finding the optimal quantity of wayside SC-based ESSs, the positioning and the sizing of each one of them, taking into account topological characteristics of the track, the LRVs timetable and the operating conditions of both the DC feeder system and the AC distribution network.

A. MATHEMATICAL FORMULATION

The sum of energy supplied by both the TPSs during the trip according to the timetable, E_{TPS}, and the energy stored by all the ESSs along the track, E_{SC}, constitutes the objective function of the proposed approach. Moreover, two penalty functions are added to the objective function. They are related to power losses and voltage drop on the AC grid to mitigate the effect of LRVs' peak power demand. The proposed optimization problem extends the methods in the existing literature by taking into account the constraints of the timetable for the railway passenger service (i.e. the LRV speed profile), the topological ones of the track, and the electrical ones of both the DC and AC networks. The decision variables are the number N of ESS on the track and the set $\vec{P}$ and $\vec{C}$ consisting of their positions and the rated values of the SC capacity, respectively:

$$\begin{aligned} \vec{P} &= [p_1, p_2, \ldots, p_n, \ldots, p_N] \\ \vec{C} &= [c_1, c_2, \ldots, c_n, \ldots, c_N] \end{aligned} \tag{20}$$

Thus, the optimization problem is formulated as follows:

$$\begin{aligned} Z : \min_{N,\vec{P},\vec{C}} \alpha \cdot E_{TPS}\left(N, \vec{P}, \vec{C}\right) + \beta \cdot E_{SC}\left(N, \vec{C}\right) + \gamma \cdot \sum_{i=1}^{N_{lines}} Z_i \\ \cdot I_i^2 + \delta \cdot \sum_{j=1}^{N_{bus}} \left| V_j^n - V_j \right| \end{aligned} \tag{21}$$

However, the relationship between E_{TPS} and the ESSs sizing and positioning along the track is not a closed-form expression. Thus, a railway system simulator is used to verify the safe operating conditions of the DC feeder system, starting from a given value of the ESSs sizing and position.

Contrariwise, E_{SC} is a closed-form expression, and it is defined as follows, where N is the number of ESSs on the track, C_n is the SC capacity of the n-th ESS, and V_{SCmax} is the maximum allowable voltage at the SC terminals.

$$\begin{aligned} E_{SC}\left(\vec{C}\right) &= \sum_{n=1}^{N} \frac{1}{2} C_n \left(V_{SCmax}^2 - \frac{1}{2} V_{SCmax}^2 \right) \\ &= \frac{1}{4} V_{SCmax}^2 \sum_{n=1}^{N} C_n \end{aligned} \tag{22}$$

In (21), the first penalty function represents the total power losses on the AC lines while the second penalty function represents the sum of voltage drops at the AC buses. However, the relationship between each of the penalty functions and the decision variables is not a closed-form expression. In particular, Z_i and I_i are the line impedance and the current rms value, at the i-th line, respectively. N_{lines} and N_{bus} are the number of lines and bus of the AC network, while V_j^n, V_j are the nominal and the present voltage values at the j-th bus, respectively. Moreover, α [-], β [-], γ [s], and δ [A · s] are weighting coefficients. An incorrect choice of the weighting coefficients significantly reduces the performance of the optimization method. In the proposed methodology, they are defined after a preliminary simulation with no ESS along the track. These results are helpful to roughly estimate the magnitude order of the energy provided by the TPS, AC power losses and AC voltage drops. In such a way, it is possible to define the weight coefficients so that all terms in

the sum representing the proposed objective function have about the same magnitude order. This is very important to avoid unbalance between the contributions in the objective function that can lead to unwanted solutions to the problem.

The optimization problem (21) is subjected to the following constraints:

$$
\begin{aligned}
1 &\leq N \leq N^{max} \\
0 &\leq p_n \leq L \quad \forall n = 1, \cdots, N \\
p_n &\leq p_{n+1} \leq L \quad \forall n = 1, \cdots, N \\
0 &\leq c_n \leq C^{max} \quad \forall n = 1, \cdots, N \\
V^{min} &\leq V_{LRV}(t) \leq V^{max} \quad \forall t \leq T \\
V^{min} &\leq V_{TPS1}(t) \leq V^{max} \quad \forall t \leq T \\
V^{min} &\leq V_{TPS2}(t) \leq V^{max} \quad \forall t \leq T \\
0 &\leq P_{TPS1}(t) \leq P^{max}_{TPS1} \quad \forall t \leq T \\
0 &\leq P_{TPS2}(t) \leq P^{max}_{TPS2} \quad \forall t \leq T \\
V^{min} &\leq V_{ESSn}(t) \leq V^{max} \quad \forall n = 1, \cdots, N \; \forall t \leq T \\
I^{min}_{SC} &\leq I_{SCn}(t) \leq I^{max}_{SC} \quad \forall n = 1, \cdots, N \; \forall t \leq T \\
V^{min}_{SC} &\leq V_{SCn}(t) \leq V^{max}_{SC} \quad \forall n = 1, \cdots, N \; \forall t \leq T \\
SoC^{min}_{SC} &\leq SoC_{SCn}(t) \leq SoC^{max}_{SC} \quad \forall n = 1, \cdots, N \; \forall t \leq T \\
SoC_{SCn}(t = T) & \\
&\geq SoC_{SCn}(t = 0) \quad \forall n = 1, \cdots, N \; \forall t \leq T \qquad (23)
\end{aligned}
$$

where N^{max} is the maximum number of ESSs along the track, L is the track length and C^{max} is the maximum value of the SC capacity for a single ESS. According to the standard BS EN 50163 and IEC 60850, V^{min} and V^{max} are the minimum and maximum allowable line voltage values (-33% and $+20\%$ of the line voltage rated value, respectively). Moreover, T is the total simulation time, P_{TPS1} and P_{TPS2} are the power supplied by the TPSs; V_{SCn}, I_{SCn}, and SoC_{SCn} are the current, voltage, and state of charge related to the n-th SC module, respectively: each one of them is limited by minimum and maximum values. The SoC isoperimetric constraint - the last equation of (21) - guarantees that energy stored by ESSs is the same at the beginning and the end of the trip cycle. Constraints related to the AC power flow regarding voltage limits at buses and current limits at branches depend on the AC network topology and characteristics, and they are considered in the AC/DC power flow procedure (Section III.C).

B. SOLUTION ALGORITHM

The proposed sizing problem is a non-linear optimization problem with real decision variables and linear constraints. It is assumed to represent it as a Mixed Integer Non-Linear Programming problem (MINLP). In fact, the problem solution depends on a line simulation implementing the non-linear models described in Section 2. For these reasons, it is not possible to solve an intractable problem, such as the proposed one, presenting no closed-form expressions, by using deterministic solution methods. Firstly, a brute-force search approach is used. Then, a hybrid genetic algorithm (GA) - particle swarm optimization (PSO) algorithm is used to explore more quickly the solutions space in order to improve its performance in terms of computing time without straining the goodness of the solution, [35]. Then, the brute-force search is used to validate the heuristic approach. Fig. 6 shows the flow chart of the solution algorithm.

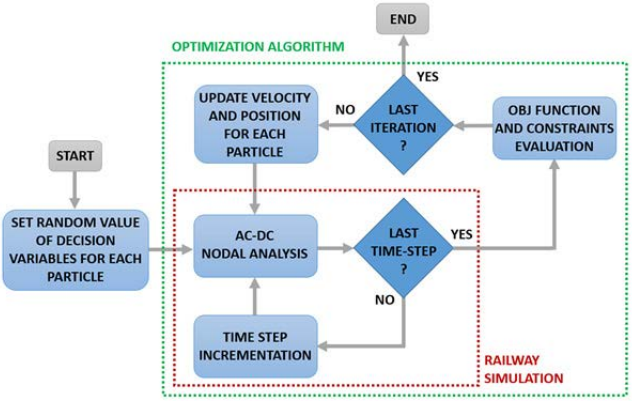

FIGURE 6. Block diagram of the ESS positioning and sizing algorithm.

After initializing the set $\vec{P}$, $\vec{C}$ and N of each particle with a random value (number, position, and capacity of the ESSs along the track), the optimization problem requires the implementation of a line simulation in which, for each time step, several DC and AC power flow are solved to perform the iterative procedure related to the AC-DC power flow. At the end of the line simulation, it is possible to compute the objective function for the specific value of the decision variables.

In each line simulation, V_{LRV} is assumed to be equal to the line voltage rated value at $t = 0$, while $P_{LRV} = I_{ESS} = 0$ at the same time step. Then, the objective function and the constraints compliance are evaluated for each particle. Finally, the position and the velocity of each particle are updated. The algorithm repeats these steps until it reaches convergence.

C. COMPUTATIONAL ANALYSIS

The Particle Swarm Optimization (PSO) performance has been compared with a Genetic Algorithm (GA) approach and Hybrid GA-PSO methodology. Although the GA method has a discrete nature and it could better approach the joint sizing and positioning problem for wayside ESSs compared the PSO, the convergence rate of the PSO method is faster than the GA method. Indeed, assuming the same number of GA chromosomes and PSO particles, the GA method is characterized by a higher risk of premature convergence to non-optimal points compared to PSO; thus, more iterations are required. Furthermore, using too many chromosomes to avoid convergence in local minimum points, the GA method requires too many evaluations of the objective function at each iteration; thus, the execution time growths and its performance are worse than those of the PSO.

In order to improve the performance of the PSO method, a hybrid GA-PSO method has been investigated [1]. The GA-PSO algorithm starts generating a random population and defines a specific number of iterations as a parameter to the algorithm. The initialized population is passed through the GA algorithm with the first half of the defined iterations. The solutions obtained from the GA algorithm are fed into the PSO algorithm with the rest of the determined iterations, to find the optimal solution from the GA-generated solutions. Through experiments, the GA-PSO algorithm's performance is the best, when the defined number of iterations is divided equally between the GA and PSO algorithms [35].

The experiments are carried out using the parameters for the optimization techniques described in the following:

GA: 20 chromosomes, uniform crossover, mutation probability 0.05, 5000 iterations.

PSO: 20 chromosomes, uniform crossover, mutation probability 0.05, 5000 iterations.

Hybrid GA-PSO: 20 chromosomes, uniform crossover, mutation probability 0.05, 20 particles, 5000 total iterations.

The weighting coefficients of the objective function α, β, γ, and δ are chosen equal to 1, 1, 10, and 100, respectively. The maximum iteration number and the threshold ν of the AC-DC power flow algorithm are imposed to 500 and 0.01, respectively. The experiment results show that the GA-PSO algorithm decreases the total execution time by about 15% compared to the PSO performance.

The computational complexity of the algorithm is not obtained using traditional methodologies because the objective of the optimization problem cannot be formulated in closed-form. However, the execution time depends mainly on the number of buses and branches of the AC network, the length of the railway line, and the time step selected for the DC power flow. As only one of these parameters increases, the execution time increases very quickly. Moreover, it is worth to note that it is not possible to define the total number of iterations for the AC-DC procedure and Hybrid GA-PSO algorithm. Indeed, as well known, the iteration number depends on the random initial conditions and the random particle updates. Thus, it is possible to provide an estimation of the algorithm's computational complexity by showing its maximum and minimum execution time using the same hardware resources. The longest and the shortest execution time for the proposed case study, evaluated on 20 runs of the optimization algorithm are 1112 seconds and 1289 seconds, respectively, using a workstation with an Intel® Core™ i7 (CPU @2.60 GHz, 64 bit) processor, 32GB of RAM, and Matlab™ R2018a.

To carry out practical large-scale simulations, it is important to consider that the main parameters that affect the increase in calculation time are the length of section L, and the number of nodes in the AC N_{bus} network. Then, it is possible to proceed and to solve the problem by means of subsequent iterations, increasing the accuracy of obtained results at each iteration. More in details, the first time the problem is solved using the proposed methodology and assuming a very large discretization step of the decision variables. Subsequently, given the optimal solution obtained in the previous step, the problem is solved again by selecting a lower discretization step and a smaller solution space for the decision variables. In fact, the solution space can be selected as small values interval centered in the value of the decision variable previously found. These steps can be repeated until the desired accuracy is reached for the solution of the problem.

TABLE 1. IEEE 7-bus RTS - power values at PQ nodes.

Node i	*P (kW)*	*Q (kVAr)*
2	30	30
3	60	30
4	20	20
5	1000	500
6	0	0
7	0	0

TABLE 2. IEEE 7-bus RTS - reactances and flow limits of the lines.

line $\ell = (i,j)$		x_ℓ (p.u.)	$f_\ell^{\max}$ (p.u.)
i	*J*		
1	2	0.0576	300
1	3	0.0920	200
2	4	0.0586	300
3	4	0.1008	150
3	6	0.1720	300
4	5	0.0625	300
5	6	0.1610	300
5	7	0.0850	300
6	7	0.0856	200

V. SIMULATION ANALYSIS

Numerical results related to the impact on the AC grid of different positioning and sizing of wayside ESS are proposed in this Section. The railway system simulator, the AC/DC iterative algorithm and the optimization algorithm are coded in MATLAB® using the MATPOWER package to solve the AC power flow.

A. CASE STUDY

Simulation tests are performed on model of the EUROPA–MOMPIANO–CASAZZA line, representing a portion of the metro network in Brescia (Italy). It consists of two sections and three stations. Two of them are located at the beginning and the end of the line, in correspondence with the TPSs, while the third one position is intermediate along the track.

Two LRVs moving in the opposite direction along the track are taken into account. They implement the same speed cycle and leave the station at the same time. Moreover, the TPSs of the DC network is assumed to be located at bus 6 and 7 of the IEEE 7-bus RTS topology shown in Fig. 7 and described in [38]. In particular, the IEEE 7-bus AC network is characterized by four constant PQ loads at bus 2, 3, 4, and 5 (Table 1) and 9 lines (Table 2); bus 1 represents the high voltage AC connection and it is selected as the slack bus. DC network is

TABLE 3. Railway system parameters.

Parameter	Value	
TRACK		
Europa-Mompiano length	592	m
Mompiano-Casazza length	1045	m
Davis formula coefficient α_1	2.7	N / kN
Davis formula coefficient α_2	0	N / (kN · km/h)
Davis formula coefficient α_3	$4 \cdot 10^{-4}$	N / (kN · km/h)^2
Von Röckl formula coefficient a	0.65	m
Von Röckl formula coefficient b	60	m
DC FEEDER SYSTEM		
Rail electric resistance	0.016	Ω/km
TPS_1 maximum power	2000	kW
TPS_2 maximum power	2000	kW
Substation DC voltage	797	V
Substation internal resistance	0.0125	Ω
TRAIN		
Loaded weight (6 passengers per m^2)	88170	kg
Rotating mass coefficient	10.46	-
Maximum traction power	630	kW
Accessories power	90	kW
Coefficient of auxiliary use	0.75	-
Wheel diameter	1040	mm
Number of motored axles	6	-
Gear-box efficiency	0.98	-
Inverter average efficiency	0.9	-
Copper loss coefficient k_c	0.3	Nm^{-2}
Iron loss coefficient k_i	0.01	s·rad^{-1}
Windage loss coefficient k_w	$5.0 \cdot 10^{-6}$	s·rad^{-3}

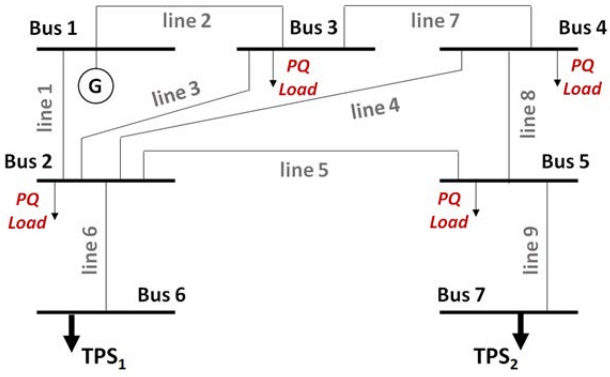

FIGURE 7. IEEE 7-bus RTS topology.

characterized by the parameters listed in Table 3. The LRV driving cycle and track elevation are shown in Fig. 8: in particular, the speed cycle consists of an acceleration phase, followed by a stretch of the path at a constant speed, and finally ending with a braking phase. Commercially available SC modules with rating voltage 125 V, nominal capacity 63 F, and weight 60 kg are assumed to be used for simulation purposes [37]. Four series SC modules compose a single ESS unit with a rating voltage of 500 V and nominal capacity of 15.75 F. The parameters of the ESS control characteristic are assumed to be $\Delta V_{SB} = 0.05$, whereas ΔV_c and ΔV_d

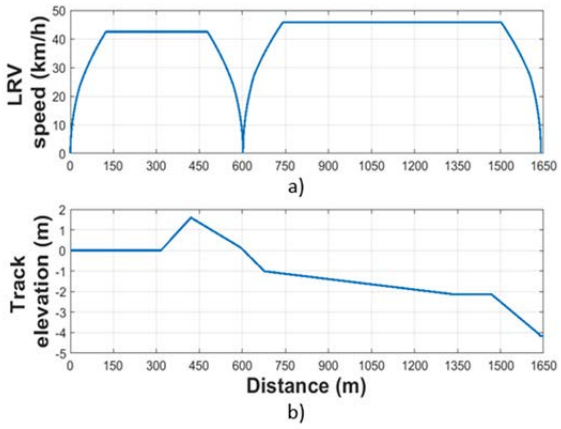

FIGURE 8. a) LRV driving cycle and b) EUROPA-CASAZZA track elevation.

are assumed to be equal to 0.33 * V_{DC} and 0.22 * V_{DC}, respectively.

B. NUMERICAL RESULTS

In the following case studies, OBESSs limited by allowable weight constraints and wayside ESSs along the track are evaluated and discussed.

case 1: no on-board or wayside ESSs.

case 2: 2 on-board ESS units (total weight 480kg).

case 3: 4 on-board ESS units (total weight 960kg).

case 4: 3 wayside ESS units at 0,25L and at 0.75L, respectively.

case 5: 2 wayside ESS units in each TPS.

case 6: optimal solution for wayside ESS sizing and positioning by using the proposed method.

The position and the capacity of the ESSs are discretized to meet real industrial requirements. Indeed, SC manufacturers produce only a few module models with different capacity values. For the proposed application, a 125V-63F SC basic module is selected, placing 4 modules in series to obtain a 500V-15.65F SC final module. For these reasons, the capacity-increasing step is assumed 15.65F (ESS unit capacity), starting from zero up to 189 F (i.e., the capacity of 12 parallel ESS units). Similarly, a 50 meters distance step for the ESS position is used, because it represents the minimum distance-increasing step, which makes it possible to highlight significant changes in the operating conditions of the DC and AC network.

A set of 2 ESSs of 63 F at 600 m and 63 F at 1550 m, respectively, represents the obtained joint sizing and positioning result of the SC-based ESSs, considering both the track directions. Figs. 9-15 show the voltages and currents on DC and AC networks, when two LRVs are moving in opposite directions from EUROPA to CASAZZA, comparing the *case 1* and *case 5*, which represent the worst case and the best case, respectively, in terms of AC and DC network operating conditions.

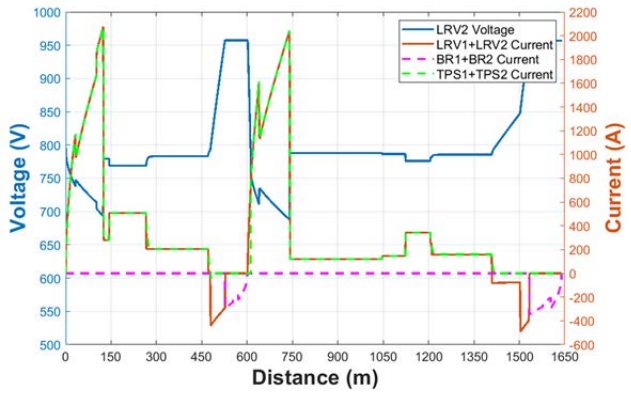

FIGURE 9. LRV e TPS voltage and current (case 1 - no ESSs).

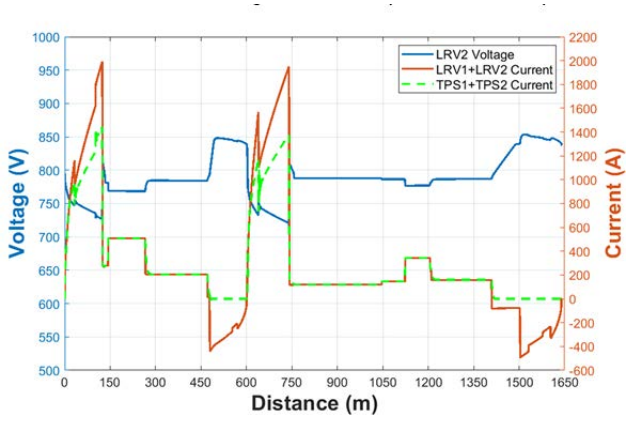

FIGURE 10. LRV e TPS voltage and current (case 5 - with ESSs).

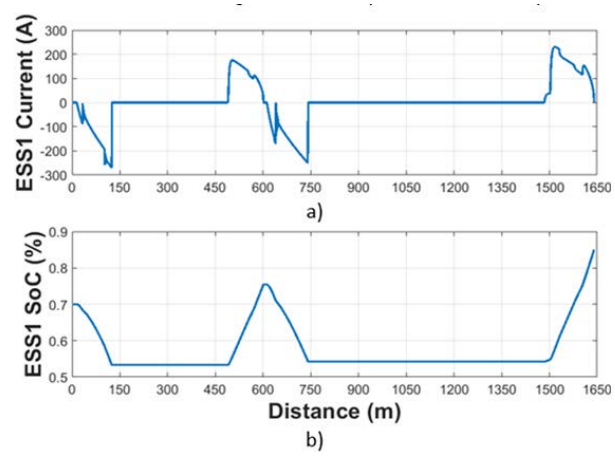

FIGURE 11. a) ESS1 DC current and, b) ESS1 SoC.

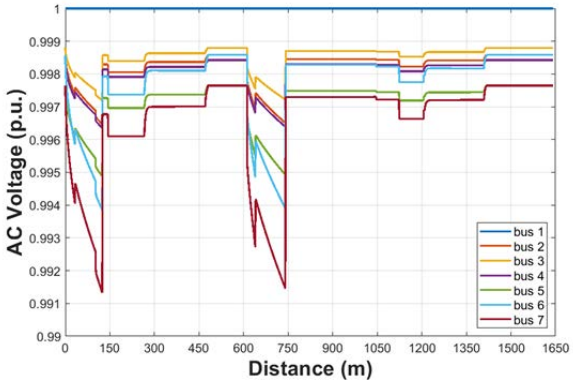

FIGURE 12. AC node voltages (case 1 - no ESSs).

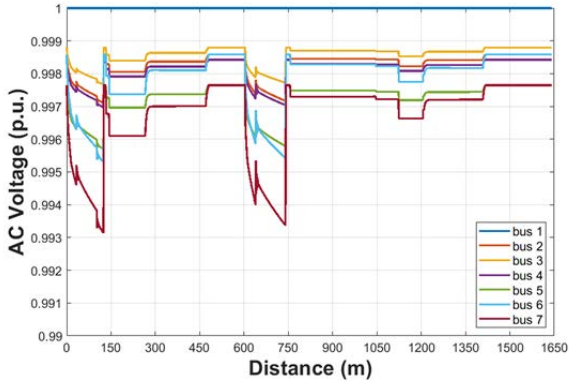

FIGURE 13. AC node voltages (case 5 - with ESSs).

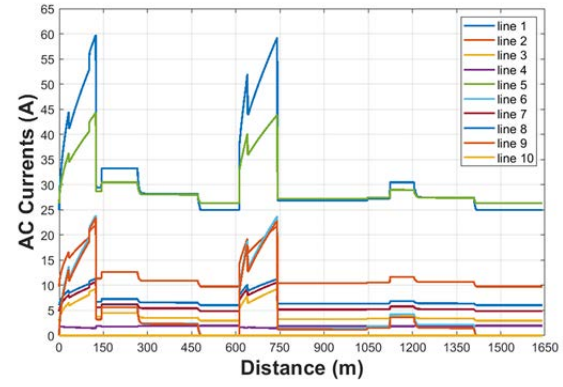

FIGURE 14. AC line currents (case 1 - no ESSs).

In particular, Fig. 9-10 show LRV voltage and current trends, highlighting the improvement of the line voltage stabilization. The ESSs are almost able to halve the voltage drops during the traction phases of the LRVs. Moreover, during the LRV regenerative braking, the ESSs keep the line overvoltage at a lower value than the protection threshold, avoiding the turn on of the braking chopper (BR) and increasing the energy efficiency of the system.

It is worth to note that the TPS and LRV current trends are overlapped, whereas a slight reduction in the LRV peak current, because in *case 5* a reduced voltage drop is obtained due to the ESSs. This is an expected result, since LRVs are modelled as constant power loads. Without loose of generality, Fig. 11 shows the ESS current and SoC trends of the SC modules for ESS1 in *case 5*.

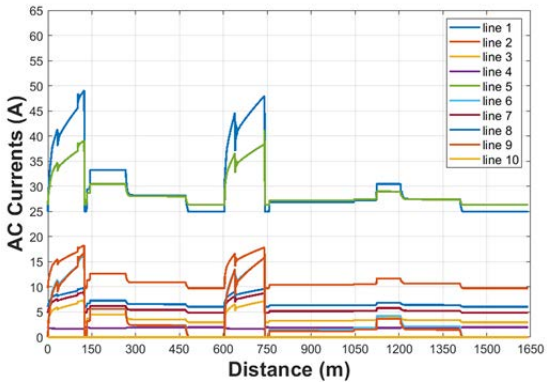

FIGURE 15. AC line currents (case 5 - with ESSs).

TABLE 4. Comparison on power losses.

	AC Network (Wh)	DC Network (Wh)	Rheostatic energy (kWh)
case 1	236.8	49.4	1.52
case 2	208.9	38.6	0.48
case 3	201.5	33.4	0.0
case 4	222.8	44,3	0.0
case 5	207.6	37.9	0.43
case 6	216.3	42.2	0.0

TABLE 5. Comparison on AC network operating conditions.

	Lines peak current (A)	Max. Nodes voltage variation (p.u.)
case 1	60.1	0.085
case 2	57.2	0.079
case 3	53.4	0.075
case 4	50.6	0.071
case 5	55.5	0.077
case 6	47.8	0.067

TABLE 6. Comparison on DC network operating conditions.

	TPS peak current (A)	TPS voltage drop (V)	Max. DC line voltage variation (%)
case 1	2083	688	+22.0
case 2	1956	700	+16.5
case 3	1798	708	+13.6
case 4	1667	713	+10.1
case 5	1943	704	+15.4
case 6	1570	726	+7.4

According to its control characteristic, the ESS1 injects current into the DC network when LRVs are powering and it absorb current to recover LRVs braking energy. The minimum SoC value is equal to 55%, while the maximum value is about 85%: these values are fully compliant with the proper operating conditions of the SC-modules. Finally, it is worth to note that the SoC values at the end of the LRV trip are greater than the SoC starting value (0.7%). In such a way, the DC network restores effective starting conditions, allowing others LRVs to move along the track.

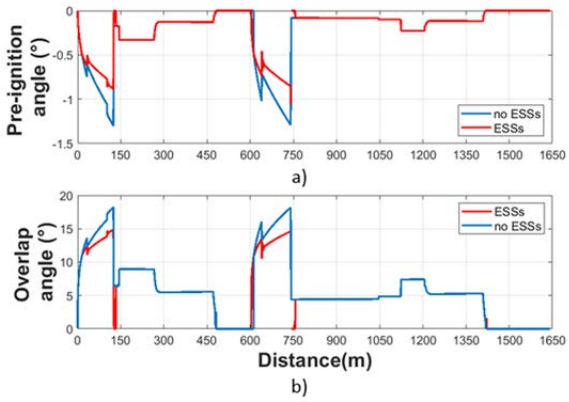

FIGURE 16. Case 1 vs. case 5 - a) TPS pre-ignition angle and b) TPS overlap angle.

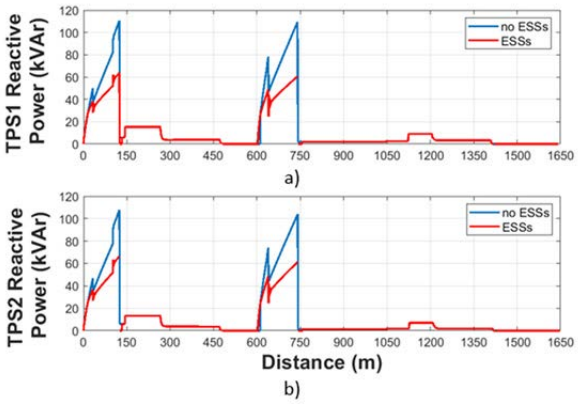

FIGURE 17. Case 1 vs. case 5 - a) TPS1 reactive power a) TPS2 reactive power.

Figs. 12-15 show AC network voltage and current trends. In particular, Figs. 12-13 compare the node voltage trends of the AC network in *case 1* and *case 5*, respectively. It is worth to note that the DC peak power supplied by the TPSs during LRVs acceleration phase is turned into voltage drop and peak current on the AC network. In particular, it affects not only the bus at which the TPS is connected, but all nodes and lines of the AC network, too. However, ESSs along the track can reduce voltage drops at AC nodes. During LRVs regenerative braking phase, the effect on the AC network of the DC overvoltage is not highlighted in the proposed analysis, because the TPSs are assumed not bidirectional.

The benefits introduced by ESSs are also shown in Figs. 14-15, comparing the AC line current trends in *case 1* and *case 5*, respectively. In fact, the peak current on the AC lines is reduced by about 17% due to ESSs along the track. However, this significant reduction in the AC line currents is related to a slight reduction in the voltage drops of the AC network nodes. This is due to the structure of the IEEE 7-bus test network that is not a geographically extensive AC network, and therefore characterized by small line impedances. Consequently, the AC line currents large variations occur with small variations of the voltage drops at the AC nodes. However, obtained results do not lose their generality and validity.

The reduction of the current peaks at the TPS AC bus bar results in a reduction of both the pre-ignition and commutation overlap angles of the three-phase rectifier, as shown in Fig 16. This reduction is followed by a reduction of the phase displacement between the AC voltage and the current of the rectifier. Consequently, it leads to an increase of the cos (φ) at the TPS MV bus bar, and then to a reduction in the reactive power flow between the TPS and the AC distribution network. In summary, the TPS reactive power is reduced because the AC line currents module is reduced and, consequently, the cos (φ) increases. Fig. 17 shows the comparison in terms of TPS reactive power in *case 1* and *case 5*. At the beginning of the traction phase, the reduction of the reactive power peak is more than 50 kVAr.

Performance comparison is summarized in Tables 4, 5, and 6 by evaluating 6 different cases. In general, the performance of the on-board ESSs (case 2 and case 3) are lower than the ones of the wayside ESSs (case 4, case 5, and case 6) for the proposed case study. More in detail, by comparing case 1 (No wayside and/or on-board ESSs) and case 6 (Sizing and positioning obtained by using the proposed methodology), the benefits obtained are significant in terms of both AC and DC network operating conditions and power losses. Moreover, by comparing case 4 (wayside ESSs located at 0.25L and 0.75L) and case 6, the TPS peak current is reduced by about 100 A and the maximum value of the DC line voltage variation is halved. Poor benefits seem to be obtained on the AC network operating conditions. This is because IEEE 7bus is not a geographically extensive network and therefore, line impedances are small, as previously stated.

Table 4 compares power losses on both DC and AC networks, and rheostatic losses are also reported. In case 1, when one LRV is breaking and no other LRVs are in the traction phase, the regenerative braking energy is entirely dissipated on a resistor. Case 2 and case 3 evaluate on-board ESSs with increased ESS capacity, respectively. Although the performance of case 2 and case 3 are better than the ones of case 1, they are lower than the cases in which wayside ESS are considered. Moreover, in case 2 the capacity of the ESS, limited by weight constraint, is not enough to avoid rheostatic losses. Considering wayside ESSs, the proposed joint sizing and positioning method for wayside ESSs allows to obtain the lowest AC and DC power losses among the various cases and to avoid rheostatic losses. More in details, Table 4 shows a comparison among the five proposed case studies in terms of power losses on both AC and DC networks. In particular, DC losses take into account power losses on the DC feeder system and the rheostatic energy wasted by LRVs during the braking; AC losses take into account power losses on the AC lines. Although case studies characterized by both OBESSs and wayside ESSs allow losses reduction on both AC and DC networks compared to the no ESSs Scenario, a greater reduction (-14.8% and -8.6% of DC and AC losses, respectively) is founded in case 3, characterized by 960 kg OBESS. Indeed, differently to wayside ESSs, OBESSs are equipped on-board the vehicle and they can support the power demand of the LRVs by avoiding power flows along the DC feeder.

Moreover, Table 5 proposes a comparison in terms of operating conditions of the AC network in terms of peak current value on the AC lines and maximum voltage variation at the AC nodes. Performance of the on-board ESSs (case 2 and case 3) are lower than in case of wayside ESSs (case 4, case 5, and case 6) for the proposed case study. In particular, case 5, related to wayside ESSs located in TPSs is characterized by performance very close to ones of case 2 and case 3. This is because the ESSs located in the TPSs are not able to effectively support the DC feeder system when LRVs are in the traction phase far from the TPSs. Although both *case 2* and *case 3* allow to reduce AC lines peak currents up to 5.2% and 11.1%, as well as AC nodes voltage drops up to 7% and 12.9%, respectively, they are not able to achieve the performance obtained in *case 4* and *case 5*. This is due to the reduced capacity of the OBESSs, which are constrained to the maximum allowed on-board weight, compared to the, not weight-constrained wayside ESSs.

Finally, Table 6 proposes a comparison in terms of operating conditions of the DC network, considering TPSs peak current values, TPSs voltage drop maximum values, and maximum voltage variation of the DC feeder system. Performance of the on-board ESSs (case 2 and case 3) are lower than case 4, case 5, and case 6 wayside ESSs for the proposed case study. In particular, the performance obtained by using the proposed method allows a reduction of the TPS peak current of about 500A compared to case 1 and about 100A compared to case 4. It is worth to note that the capacity of wayside ESSs in case 6, being able to avoid the switch on of the breaking chopper, allows to obtain the best performances in reducing the maximum voltage variation on the DC feeder system (about 15% compared to case 1). More in details, Table 6 shows a significant reduction (about 20% for *case 5*) of TPS supplied peak current, resulting in a great saving on the sizing of the TPS power converters. Moreover, the maximum line voltage variation in *case 5* is much lower (about 7.4%) compared to *case 1*. ESSs significantly reduce voltage risings. Furthermore, they hold the line voltage at a much lower value than the allowable maximum limit, avoiding the activation of the braking chopper.

It is worth to note that performances do not improve if the distance between ESSs and the train station increases: instead, best results are obtained when the ESS is installed very close to the track position at which the LRV starts the traction phase or the braking phase. In such a way, it is possible to minimize the voltage drop or voltage rise, and the power losses on the feeder system are also minimized at the same time.

To the best of Authors knowledge, there are no other ESS sizing and positioning methods taking into account the AC network operating constraints. However, Table 7 compares different methodologies in order to show the effectiveness of the proposed approach. In detail, the proposed method is compared with the particular case in which $\gamma = \delta = 0$

TABLE 7. Comparison between different ESS design methods.

	TPS voltage drop (V)	Max. Nodes voltage variation (p.u.)
Proposed method	726	0.067
γ=δ=0 method, [17]	731	0.079
Literature method, [39]	728	0.082

(i.e. the penalty functions are not considered), and a method in technical literature considering only one wayside ESS for each section of the track to mitigate the voltage drop on the DC network [17].

The third method is aimed at minimizing the following objective function, considering the squared difference between the LRV voltage and the rated line voltage [39].

$$\int_0^T (V_{LRV}(t) - V_{DC})^2 \, dt \tag{24}$$

The capacity and the position of the ESS are assumed as decision variables. Although the second and third methods are more effective to reduce voltage drops and power losses on the DC feeder system, the first method also allows to mitigate the effect of the LRV peak power demand on the AC grid, since the constraints related to its operating conditions are also taken into account.

In summary, the wayside ESS sizing and positioning problem is a very complex task due to the strong non-linearity aspects characterizing this problem. Moreover, it depends on the topological characteristics of the track and the LRV speed profile, so that it cannot be expressed through a mathematical closed-form relationship. For these reasons, general principles for the ESS design and positioning along the track cannot be provided. Thus, it is required to use proper simulation tools, such as the one proposed in this paper, to analyse the specific case study. However, it is a good design rule to place wayside ESS very close to the distance along the track where LRV accelerations and/or brakes are expected because they could cause voltage drops and rises. However, the topological characteristics of the track and both the DC and AC networks operating conditions can significantly affect design solutions, requiring ESS positioning and sizing that can disagree with this general rule. For example, it could not be useful to locate one ESS at a distance where one LRV accelerates on a downhill track section, because it can cause a limited voltage drop. Otherwise, when LRV speed profiles are characterized by several acceleration phases, is not useful to place the ESS at a distance where the LRV is in its first acceleration phase, because its related voltage drop can be mitigated by the close traction substation. Instead, following LRV accelerations might require an optimal design solution to install one or more ESS due to the distance from the closest TPS. Moreover, the complexity of the wayside ESS sizing and positioning problem has been further increased by also taking into account aspects related to voltage drops and peak currents on buses and branches of the AC distribution network.

Finally, although the OBESSs allow to obtain the lowest power losses on DC network, the performance in terms of voltage drop reduction to the AC network buses is lower than in case of wayside ESS, due to the smaller size imposed by weight constraints. As a general remark, it follows that OBESSs allow LRVs to obtain functionalities such as recovery of regenerative braking energy, catenary-free running, and reduction of peak power consumption. Wayside ESSs, on the other hand, can provide OBESS functionalities (except for catenary-free running) and significantly mitigate the impact of the railway DC feeder working conditions on the AC grid.

However, the effectiveness of OBESS and wayside ESSs have to be analysed and compared by performing techno-economic evaluations in each particular case study.

VI. CONCLUSION

In the paper, it is investigated the impact on the AC bus voltages and branch currents of wayside SC-based ESSs supporting the DC railway system. In particular, the DC railway system is modeled a simulation tool for solving the decoupled AC/DC power flow taking into account the 3-phase bridge rectifier of the TPS is implemented. Moreover, it is proposed a novel mathematical formulation of the optimization problem for the positioning and sizing of SC-based ESSs. The wayside ESS sizing and positioning problem is a very complex task due to the strong non-linearity aspects characterizing this problem. Moreover, it depends on the topological characteristics of the track and the LRV speed profile, so that it cannot be expressed through a closed-form mathematical relationship. For these reasons, general principles for the ESS design and positioning along the track cannot be provided and it is required to use proper simulation tools, such as the one proposed in the paper, to analyse each specific case study.

Obtained simulation results based on the EUROPA-CASAZZA Italian DC metro network show benefits in terms of energy efficiency and operating conditions on the DC and AC network, respectively. In fact, SC-based ESS installed along the track allows to reduce AC power losses up to 8.6%. On the other hand, it significantly reduce peak current and the voltage drop on the AC grid due to the LRVs accelerations. More in detail, lines peak currents are reduced up to 11.1%, while voltage drops at nodes are also reduced up to 12.9%, decreasing, therefore, the total harmonic distortion on the grid. A reduction in the reactive power flow between the TPS and the AC distribution network is also highlighted.

Finally, assuming SC-based ESSs, the performance in terms of voltage drop reduction to the AC network buses of the OBESSs is lower than that ones of wayside ESS. However, the effectiveness of OBESS and wayside ESSs must be analyzed and compared by performing techno-economic evaluations in each particular case study.

Future research directions will deal with the performance comparison of different ESS technologies (e.g. batteries,

flywheels, etc.) and ESS control strategies. Moreover, the analysis proposed in the paper could be useful for a techno-economic analysis aimed at evaluating and comparing the benefits of ESSs on both AC and DC networks.

REFERENCES

[1] International Transport Forum (ITF). (2017). *ITF Transport Outlook 2017*. [Online]. Available: https://read.oecd-ilibrary.org/transport/itf-transport-outlook-2017_9789282108000-en#page13

[2] International Energy Agency (IEA). (2018). *World Energy Outlook*. [Online]. Available: https://www.iea.org/weo2018/

[3] International Energy Agency (IEA). (2017). *Railway Handbook 2017–Energy Consumption and CO2 Emissions*. [Online]. Available: http://www.sipotra.it/wp-content/uploads/2018/03/Railway-Handbook-2017-Energy-Consumption-and-CO2-Emissions.-Focus-on-Passenger-Rail-Services.pdf

[4] International Union of railways (UIC). (2016). *Technologies and Potential Developments for Energy Efficiency and CO2 Reductions in Rails Systems*. [Online]. Available: http://uic.org/IMG/pdf/_27_technologies_and_potential_developments_for_energy_efficiency_and_co2_reductions_in_rail_systems._uic_in_colaboration.pdf

[5] Z. Li, S. Hoshina, N. Satake, and M. Nogi, "Development of DC/DC converter for battery energy storage supporting railway DC feeder systems," *IEEE Trans. Ind. Appl.*, vol. 52, no. 5, pp. 4218–4224, Sep./Oct. 2016.

[6] R. Barrero, X. Tackoen, and J. Van Mierlo, "Quasi-static simulation method for evaluation of energy consumption in hybrid light rail vehicles," in *Proc. IEEE Vehicle Power Propuls. Conf.*, Sep. 2008, pp. 1–7.

[7] S. Yang, L. R. Zhigang Anders, N. Petter, and L. Zhendong, "Contact wire irregularity stochastics and effect on high-speed railway pantograph–catenary interactions," *IEEE Trans. Instrum. Meas.*, vol. 69, no. 10, pp. 8196–8206, Oct. 2020.

[8] N. Ghaviha, J. Campillo, M. Bohlin, and E. Dahlquist, "Review of application of energy storage devices in railway transportation," *Energy Proc.*, vol. 105, pp. 4561–4568, May 2017.

[9] A. Capasso, R. Lamedica, A. Ruvio, M. Ceraolo, and G. Lutzemberger, "Modelling and simulation of electric urban transportation systems with energy storage," in *Proc. IEEE 16th Int. Conf. Environ. Electr. Eng. (EEEIC)*, Jun. 2016, pp. 1–6.

[10] G. Graber, V. Galdi, V. Calderaro, and A. Piccolo, "Sizing and energy management of on-board hybrid energy storage systems in urban rail transit," in *Proc. Int. Conf. Electr. Syst. Aircr., Railway, Ship Propuls. Road Vehicles Int. Transp. Electrific. Conf. (ESARS-ITEC)*, Nov. 2016, pp. 1–6.

[11] H. Takahashi, Y. Kume, K. Honda, H. Kawatsu, J. Kaminishi, and Y. Shimizu, "Development of emergency self-running train for energy utilization in stationary energy storage system," in *Proc. 17th Eur. Conf. Power Electron. Appl. (EPE ECCE-Europe)*, Sep. 2015, pp. 1–8.

[12] A. Rufer, D. Hotellier, and P. Barrade, "A supercapacitor-based energy storage substation for voltage compensation in weak transportation networks," *IEEE Trans. Power Del.*, vol. 19, no. 2, pp. 629–636, Apr. 2004.

[13] A. M. Gee and R. W. Dunn, "Analysis of trackside flywheel energy storage in light rail systems," *IEEE Trans. Veh. Technol.*, vol. 64, no. 9, pp. 3858–3869, Sep. 2015.

[14] M. Sadakiyo, N. Nagaoka, A. Ametani, S. Umeda, Y. Nakamura, and J. Ishii, "An optimal operating point control of lithium-ion battery in a power compensator for DC railway system," in *Proc. 42nd Int. Universities Power Eng. Conf.*, Sep. 2007, pp. 681–686.

[15] F. Ciccarelli, D. Iannuzzi, K. Kondo, and L. Fratelli, "Line-voltage control based on wayside energy storage systems for tramway networks," *IEEE Trans. Power Electron.*, vol. 31, no. 1, pp. 884–899, Jan. 2016.

[16] H. Hayashiya, D. Hara, and M. Tojo, "Lithium-ion battery installation in traction power supply system for regenerative energy utilization: Initial report of effect evaluation after half a year operation," in *Proc. 16th Int. Power Electron. Motion Control Conf. Expo.*, Antalya, Turkey, Sep. 2014, pp. 119–124.

[17] V. Calderaro, V. Galdi, G. Graber, and A. Piccolo, "Optimal siting and sizing of stationary supercapacitors in a metro network using PSO," in *Proc. IEEE Int. Conf. Ind. Technol. (ICIT)*, Mar. 2015, pp. 1–6.

[18] H. Hayashiya, Y. Iino, H. Takahashi, K. Kawahara, T. Yamanoi, T. Sekiguchi, H. Sakaguchi, A. Sumiya, and S. Kon, "Review of regenerative energy utilization in traction power supply system in Japan: Applications of energy storage systems in D.C. traction power supply system," in *Proc. 43rd Annu. Conf. IEEE Ind. Electron. Soc. (IECON)*, Oct. 2017, pp. 3918–3923.

[19] M. Chymera, A. C. Renfrew, and M. Barnes, "Railway modelling for power quality analysis," in *WIT Transactions on The Built Environment*, vol. 88. WIT Press, 2006, pp. 1–8. [Online]. Available: https://witpress.com/elibrary/wit-transactions-on-the-built-environment/88/16680

[20] C. L. Pires, S. I. Nabeta, and J. R. Cardoso, "DC traction load flow including AC distribution network," *IET Electr. Power Appl.*, vol. 3, no. 4, pp. 289–297, Jul. 2009.

[21] F. Hao, G. Zhang, J. Chen, Z. Liu, D. Xu, and Y. Wang, "Optimal voltage regulation and power sharing in traction power systems with reversible converters," *IEEE Trans. Power Syst.*, vol. 35, no. 4, pp. 2726–2735, Jul. 2020.

[22] C. V. Pathak and D. Makwana, "Power quality improvement in railway traction system," *Int. J. Technol. Res. Eng.*, vol. 3, no. 9, pp. 2347–4718, May 2016.

[23] *IEEE Recommended Practices and Requirements for Harmonic Control in Electrical Power Systems*, IEEE Standard 519-1992, 1992. [Online]. Available: https://edisciplinas.usp.br/pluginfile.php/2587623/mod_resource/content/2/IEEE-519-1992.pdf

[24] S. M. M. Gazafrudi, A. T. Langerudy, E. F. Fuchs, and K. Al-Haddad, "Power quality issues in railway electrification: A comprehensive perspective," *IEEE Trans. Ind. Electron.*, vol. 62, no. 5, pp. 3081–3090, May 2015.

[25] G. Graber, V. Galdi, V. Calderaro, A. Piccolo, and L. Fratelli, "Experimental validation of a steady-state metro network simulator for eco-drive operations," in *Proc. IEEE 16th Int. Conf. Environ. Electr. Eng. (EEEIC)*, Jun. 2016, pp. 1–6.

[26] L. Battistelli, P. Caramia, G. Carpinelli, D. Lauria, and D. Proto, "A power quality compensation device for interacting AC-DC railway systems," in *Proc. IEEE Russia Power Tech*, Jun. 2005, pp. 1–6.

[27] K. Wang, Q. Ge, and Y. Li, "Analysis and optimized control of emergency traction by storage battery for urban rail transit vehicle," in *Proc. 17th Int. Conf. Electr. Mach. Syst. (ICEMS)*, Oct. 2014, pp. 175–179.

[28] F. Perticaroli, *Sistemi Elettrici Per I Trasporti*, 2nd ed. New Delhi, India: CEA, 2001.

[29] G. Graber, V. Calderaro, V. A. R. Galdi Piccolo Lamedica, and A. Ruvio, "Techno-economic sizing of auxiliary-battery-based substations in DC railway systems," *IEEE Trans. Transp. Electrific.*, vol. 4, no. 2, pp. 616–625, Jun. 2018.

[30] A. Mahmoudi, W. L. Soong, G. Pellegrino, and E. Armando, "Efficiency maps of electrical machines," in *Proc. IEEE Energy Convers. Congr. Expo. (ECCE)*, Sep. 2015, pp. 2791–2799.

[31] D. J. Tylavsky and F. C. Trutt, "Terminal behaviour of the uncontrolled R-L fed 3-phase bridge rectifier," *IEE Proc. B-Electr. Power Appl.*, vol. 129, no. 6, pp. 337–343, Nov. 1982.

[32] Y.-S. Tzeng, N. Chen, and R.-N. Wu, "A detailed R-L fed bridge converter model for power flow studies in industrial AC/DC power systems," *IEEE Trans. Ind. Electron.*, vol. 42, no. 5, pp. 531–538, Oct. 1995.

[33] S. Chenh, M. Sautreuil, D. Riu, and N. Retiere, "Quasi-static decoupled load flow modelling of a power supply network with AC-DC converters applied to light rail system," in *Proc. Eur. Conf. Power Electron. Appl.*, 2007, pp. 1–10.

[34] H. M. A. Ahmed, A. B. Eltantawy, and M. M. A. Salama, "A generalized approach to the load flow analysis of AC–DC hybrid distribution systems," *IEEE Trans. Power Syst.*, vol. 33, no. 2, pp. 2117–2127, Mar. 2018.

[35] Y. Valle, G. K. Venayagamoorthy, S. Mohagheghi, J. C. Hernandez, and R. G. Harley, "Particle swarm optimization: Basic concepts, variants and applications in power systems," *IEEE Trans. Evol. Comput.*, vol. 12, no. 2, pp. 171–195, Apr. 2008.

[36] A. M. Manasrah and H. Ba Ali, "Workflow scheduling using hybrid GA-PSO algorithm in cloud computing," *Wireless Commun. Mobile Comput.*, vol. 2018, Jan. 2018, Art. no. 1934784.

[37] Maxwell Technologies. (2019). *Ultracapacitors Module 125 V*. [Online]. Available: http://www.maxwell.com/images/documents/125V_Module_datasheet.pdf

[38] J. Contreras, R. C. Garcia, J. B. C. Garcia, and M. van Akkeren, "A binomial tree model for investment in transmission assets," *Int. J. Electron. Bus. Manage.*, vol. 5, no. 3, pp. 163–172, Jan. 2007.

[39] T. Ratniyomchai, S. Hillmansen, and P. Tricoli, "Optimal capacity and positioning of stationary supercapacitors for light rail vehicle systems," in *Proc. Int. Symp. Power Electron., Electr. Drives, Autom. Motion*, Jun. 2014, pp. 807–812.

G. GRABER (Member, IEEE) received the M.Sc. degree in electronic engineering and the Ph.D. degree in information engineering from the University of Salerno, Italy, in 2011 and 2016, respectively. He is currently a Research Fellow and collaborates with the Department of Industrial Engineering, University of Salerno. His main research interests include innovative solutions for increasing energy efficiency in railway systems and impact assessment of electric vehicles charging demand and storage systems in smart grids.

V. CALDERARO (Senior Member, IEEE) received the M.Sc. degree in electronic engineering and the Ph.D. degree in information engineering from the University of Salerno, Italy, in 2001 and 2006, respectively. He is currently an Assistant Professor with the Department of Industrial Engineering. His current research interests include integration of distributed generation and storage systems on electrical distribution networks, soft computing methodologies in power system applications, and protection and diagnosis of complex systems.

V. GALDI (Senior Member, IEEE) received the M.Sc. degree in electronic engineering from the University of Salerno, Italy, in 1994, and the Ph.D. degree in electrical engineering from the University of Napoli, Italy, in 1999. Since 2018, he has been a Full Professor at the University of Salerno. His current research interests include ICT application to power systems, power management and energy efficiency in transportation systems, smart grids, energy storage systems, and ITS.

L. IPPOLITO received the M.Sc. degree in electronic engineering from the University of Salerno, Italy, in 1992, and the Ph.D. degree in electrical engineering from the University of Napoli, Italy, in 1997. Since 2001, he has been an Associate Professor at the University of Salerno. He has longstanding interest in renewable energy and his current research interests include smart grids, energy efficiency, and green hydrogen technologies.

G. MASSA (Member, IEEE) received the M.Sc. degree in electronic engineering and the Ph.D. degree in electronic engineering and computer science from the University of Salerno, Fisciano, Italy, in 2009 and 2013, respectively. He has been working for various companies, mainly as a smart grid specialist and a project engineer. His main research interests include distributed generation systems, soft computing methodologies in power system applications, energy saving in electric transportation, and Industry 4.0 technologies for advanced O&M of renewable energy-based power plants.